THE JOURNAL OF PHYSICAL CHEMISTRY Letters

Letter

Cite This: J. Phys. Chem. Lett. 2020, 11, 419−426

pubs.acs.org/JPCL

Implementation of Geometry-Dependent Charge Flux into the Polarizable AMOEBA+ Potential

Chengwen Liu,[†] Jean-Philip Piquemal,[†,‡,§] and Pengyu Ren*,[†]

[†]Department of Biomedical Engineering, The University of Texas at Austin, Austin, Texas 78712, United States

[‡]Laboratoire de Chimie Théorique, Sorbonne Université, UMR7616 CNRS, 75252 Paris, France

[§]Institut Universitaire de France, 75005, Paris, France

Supporting Information

ABSTRACT: Molecular dynamics (MD) simulations employing classical force fields (FFs) have been widely used to model molecular systems. The important ingredient of the current FFs, atomic charge, remains fixed during MD simulations despite the atomic environment or local geometry changes. This approximation hinders the transferability of the potential being used in multiple phases. Here we implement a geometry-dependent charge flux (GDCF) model into the multipole-based AMOEBA+ polarizable potential. The CF in the current work explicitly depends on the local geometry (bond and angle) of the molecule. To our knowledge, this is the first study that derives energy and force expressions due to GDCF in a multipole-based polarizable FF framework. Due to the inclusion of GDCF, the AMOEBA+ water model is noticeably improved in terms of describing the monomer properties, cluster binding/interaction energy, and a variety of liquid properties, including the infrared spectra that previous flexible water models were not able to capture.

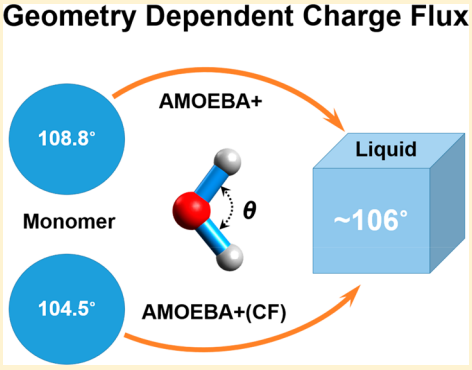

Classical force fields (FFs) are commonly used to describe inter- and intramolecular interactions in molecular dynamics (MD) simulations. In popular point charge FFs, the atomic charges remain fixed during simulations. It is well understood however how charge distributions are affected by both chemical environments through polarization effect and local geometry changes.[1] The former is explicitly treated in "polarizable" FFs such as the Drude oscillator,[2] atomic induced dipole,[3] and fluctuating charge models, where the charges can be calculated from the energy equilibration,[4−6] or the bond capacity model.[7] The latter is ignored by almost all classical FFs even though it is well-known that it causes issues. For example, the HOH angle of water in gas (104.5),[8] liquid (∼106),[9] and ice (∼109.5°)[10] cannot be described consistently by common flexible model models.[11,12] This is due to incorrect dipole derivative of these flexible water models, without accounting for intramolecular charge transfer or charge flux (CF) when the water geometry changes. The spectroscopically determined force field (SDFF) electrostatics by Krimm and co-workers is one of the few FFs that adopt a CF contribution.[13−15] Their study showed that CF is not only the key to the water angle opening from an isolated water molecule to its liquid phase but also helps in describing the conformational potential energy surface of the peptide.[13] TTM-family models by Xantheas and co-workers are other examples that incorporate CF effect.[16,17] Both the SDFF and TTM models show the necessity of incorporating CF for successfully describing vibrational spectroscopy, which requires an accurate description of the molecular dipole surface.[11,13−17] Dinur pointed out that CF is a first-order contribution to the electrostatic force in general and should not be neglected in MD simulations for flexible molecules.[12] Dinur and Hagler proposed a geometry-dependent charge flux (GDCF) model, where atomic charges are explicitly dependent on the local geometry (bond, angle, and torsion), for a series of small organic molecules. On the basis of the molecular dipole moments of organic molecules and amino acids calculated with density functional theory and point charge FFs, Sedghamiz et al. concluded that the majority (∼85%) of the conformational dependence of molecular dipole moments can be attributed to the pure geometry effect and the remainder should be explicitly modeled by the GDCF model.[18,19] Thus, they suggested an inclusion of CF contribution from bonds, angles, and dihedrals for developing more transferable FFs. By contrast, Dinur and Hagler demonstrated that CF due to bonds and angles is much more significant than that from dihedrals.[20]

The AMOEBA (Atomic Multipole Optimized Energetics for Biomolecular Applications) FF uses multipoles up to quadrupole to describe electrostatics and induced dipoles to capture the nonadditive many-body effect.[3,21−24] The AMOEBA+ potential was developed very recently, where the "short-range" physics including charge penetration[25] and intermolecular charge transfer[26] effects were incorporated. In addition, in the AMOEBA+ model, the original Thole polarization model

Received: November 25, 2019
Accepted: December 22, 2019
Published: December 23, 2019

DOI: 10.1021/acs.jpclett.9b03489
J. Phys. Chem. Lett. 2020, 11, 419−426

(direct component)[27−29] was improved to better capture the MP2 many-body energy of molecular clusters, along with better combining rules for the empirical van der Waals potential.[30] Nevertheless, the atomic charge (monopole) in the AMOEBA+ model is still independent of the local geometry changes. Consequently, similar to the current AMOEBA model and other flexible water models, an artificially large equilibrium HOH angle of 108.8° was used in AMOEBA+ in order to reach the correct bending angle in the liquid phase (~106°). As mentioned above, it has been well recognized that this is attributed to the fact that the molecular charge distribution cannot properly adjust to the changing geometry, i.e., dipole derivatives are incorrect. In this work, we implement the GDCF model into the AMOEBA+ potential. Different from the model proposed by Dinur and Hagler,[20] only the CFs along bond and angle contributions are considered. In addition, we systematically integrated the GDCF model with permanent and polarizable multipole interactions, with analytical gradients. With CF inclusion, the previous AMOEBA+ water model was reparametrized using the ForceBalance toolkit[31] by targeting both gas-phase QM data and liquid-phase observables, resulting in the current AMOEBA+(CF) water model.

To use a water molecule as an illustration (Figure 1), CF along each bond is described as a function of the deviation of

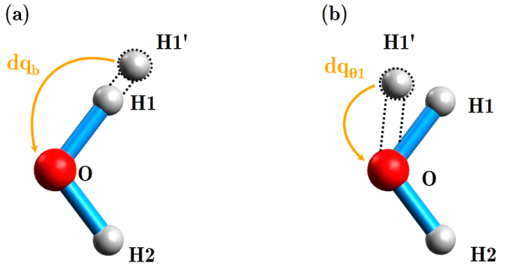

Figure 1. Schematic illustration of the GDCF model. (a) CF due to bond stretching and (b) CF due to angle bending, where dq_b and $dq_{\theta 1}$ represent the absolute CFs due to bond stretching and angle bending. The direction (sign) of CF is defined in the Methodologies section.

bonds and angles from their equilibrium values. For water, the experimental angle and bond length (104.5° and 0.9572 Å) are used as the reference. The CF direction rules are kept the same as those suggested by Dinur and Hagler.[20] The CF on each atom is added to its permanent monopole values prior to energy and force computations. Derivation of the GDCF model in the AMOEBA+ framework, including the permanent multipole and polarization energy and forces, is detailed in the Methodologies section and Supporting Information (SI). The newly parametrized AMOEBA+(CF) water model is extensively compared with the previous AMOEBA+ and other advanced water models. Below, to clearly demonstrate the improvement due to the inclusion of GDCF, we systematically report the results of the new water model from the monomer to clusters and to liquid properties.

Water Monomer Properties. As mentioned above, GDCF potentially leads to the automatic angle opening in liquid-phase simulations of water. This allows us to use an angle of experimental geometry as the initial parameter. As shown in Table 1, AMOEBA+(CF) angle and bond final parameters (after cluster/liquid refinement) resemble the experimental values of an isolated water molecule. The force constants of

Table 1. Vibrational Frequencies and Geometrical and Moment Properties of an Isolated Water Molecule[a]

property		experiment[c]	AMOEBA +[d]	AMOEBA +(CF)[e]
vibrational frequency[b] (cm^{-1})	ν_{ss}	3657	**3658**	**3656**
	ν_{as}	3756	**3757**	**3755**
	ν_b	1595	1627	**1594**
geometry	b_{OH} (Å)	0.957	0.939	**0.950**
	θ_{HOH} (deg)	104.52	108.82	**104.54**
dipole (Debye)	d_z	1.86 (1.84)	1.95	**1.88**
quadrupole (Debye·Å)	Q_{xx}	2.63 (2.57)	3.17	**2.83**
	Q_{yy}	−2.50 (−2.42)	−2.69	**−2.34**
	Q_{zz}	−0.13 (−0.14)	**−0.48**	−0.49
polarizability ($Å^3$)	α_{xx}	1.53 (1.47)	**1.59**	1.62
	α_{yy}	1.42 (1.38)	1.21	**1.24**
	α_{zz}	1.47 (1.42)	1.33	**1.36**

[a]Values in bold indicate a better consistency with the experimental data. [b]ν_{ss}: symmetrical stretching; ν_{as}: asymmetrical stretching; ν_b: bending vibration. [c]Experimental data were taken from references: vibrational frequencies,[32] geometry,[32] dipole,[33] quadrupole,[34] and polarizability;[35] values in parentheses are ab initio data taken from ref 36. [d]Calculated with the AMOEBA+-optimized monomer geometry [e]Calculated with the AMOEBA+(CF)-optimized monomer geometry.

bonded terms are adjusted slightly to better describe the experimental vibration frequencies of an isolated monomer. In addition, using the minimal-energy geometry, we show that the quality of the molecular dipole, quadrupole, and polarizability is significantly improved over those of the AMOEBA+ model, which has compensative bigger dipole and quadrupole moments but smaller molecular polarizability. Early AMOEBA models are not shown here, but they are quite similar to AMOEBA+. As expected, the final/optimal nonbonded parameters change only in small fraction compared to those of the AMOEBA+ model (Table S1).

Water Dimer Properties. Both the binding energy (BE, eq 1) and interaction energy (IE, eq 2) were computed. The former used optimized monomers as references to keep the monomer's geometry the same as that in the dimer geometry. The dissociation energy (negative of BE) of the canonical hydrogen-bonding water dimer from the AMOEBA+(CF) model was 4.87 kcal/mol, which is slightly improved comparing to that from AMOEBA+ (4.81 kcal/mol) and in agreement with the CCSD(T)/CBS[37] value of 4.98 kcal/mol. In addition, the AMOEBA+(CF) predicts intermolecular IE components, including electrostatics, induction, and van der Waals, matching those from the SAPT2+ model (Figure S1). Besides the canonical hydrogen-bonding dimer, the "Smith dimers"[38] formed through different directional hydrogen bonds often serve as model dimers to examine the anisotropy of water models. AMOEBA+(CF) predicts the BE of 10 Smith dimers extremely well with an RMSE of 0.25 kcal/mol compared to that of 0.59 kcal/mol of the AMOEBA+ model. As an additional comparison, the results from the MB-UCB water model,[39] which shares many similarities with the AMOEBA+ model, are also provided in Table 2.

$$\Delta E_{\text{binding}} = E^{\text{opt}}_{\text{dimer}} - 2E^{\text{opt}}_{\text{monomer}} \quad (1)$$

$$\Delta E_{\text{interaction}} = E_{\text{dimer}} - E^{*}_{\text{monomer1}} - E^{*}_{\text{monomer2}} \quad (2)$$

DOI: 10.1021/acs.jpclett.9b03489
J. Phys. Chem. Lett. 2020, 11, 419−426

Table 2. BEs (with MP2-Optimized Geometry) of Smith Dimers Predicted by Several Water Models Compared to CCSD(T)/CBS Data[a]

structure	CCSD(T)/CBS[bc]	AMOEBA+[bd]	AMOEBA +(CF)[b]	MB-UCB[e]
Smith01	−4.97	−5.42 (−4.96)	**−4.98**	−5.15
Smith02	−4.45	−4.57 (−4.11)	**−4.37**	−4.78
Smith03	−4.42	−4.45 (−4.00)	**−4.29**	−3.86
Smith04	−4.25	−5.20 (−4.75)	**−4.09**	−3.11
Smith05	−4.00	−4.53 (−4.08)	−3.53	**−3.68**
Smith06	−3.96	−4.36 (−3.90)	**−3.38**	−3.21
Smith07	−3.26	−4.15 (−3.69)	**−3.19**	−2.93
Smith08	−1.30	−1.85 (−1.39)	**−1.38**	−1.15
Smith09	−3.05	−3.67 (−3.22)	**−3.03**	−2.99
Smith10	−2.18	−2.79 (−2.34)	**−2.27**	−2.07
RMSE		0.59 (0.28)	**0.25**	0.51

[a]All energies are in kcal/mol. [b]BEs using MP2-optimized geometry for the dimer and monomer.[31,38] [c]CCSD(T)/CBS values were taken from ref 40. [d]Values in parentheses are BEs using the MP2-optimized dimer and experimental monomer. These values were reported in the previous AMOEBA+ publication.[26] [e]These values were taken from ref 39.

In the above equations, superscripts opt means optimized geometry, and * means monomer geometry kept the same as that in dimer.

Larger Water Clusters. We demonstrate here that the AMOEBA+(CF) model is capable of accurately predicting both the BEs and IEs for large water clusters from the trimer to 17-mers compared to available CCSD(T)/CBS data. Here the BEs of water models were calculated from the FF-optimized geometry, while the CCSD(T)/CBS used the MP2-optimized geometry. The IEs were calculated using the MP2-optimized cluster geometry for both the QM and FFs. As seen from Figure 2a–c for BEs for clusters from the trimer to 17-mers, MB-UCB and AMOEBA+ give overall RMSEs of 2.95 and 1.89 kcal/mol, respectively. The AMOEBA+(CF) model remarkably reduces the error to 0.67 kcal/mol (Table S2). For the IEs of tetra-, penta-, and hexamer isomers, the AMOEBA+ model gives an RMSE of 1.74 kcal/mol, and AMOEBA+(CF) significantly reduces the error to 0.36 kcal/mol, which is slightly better than MB-pol water model (0.39 kcal/mol) (Table S3). It is worth mentioning that the MB-pol model was explicitly fitted on the IEs of water clusters,[41] while only the BEs were included as the targets in AMOEBA+(CF) parametrization (in addition to selected liquid properties).

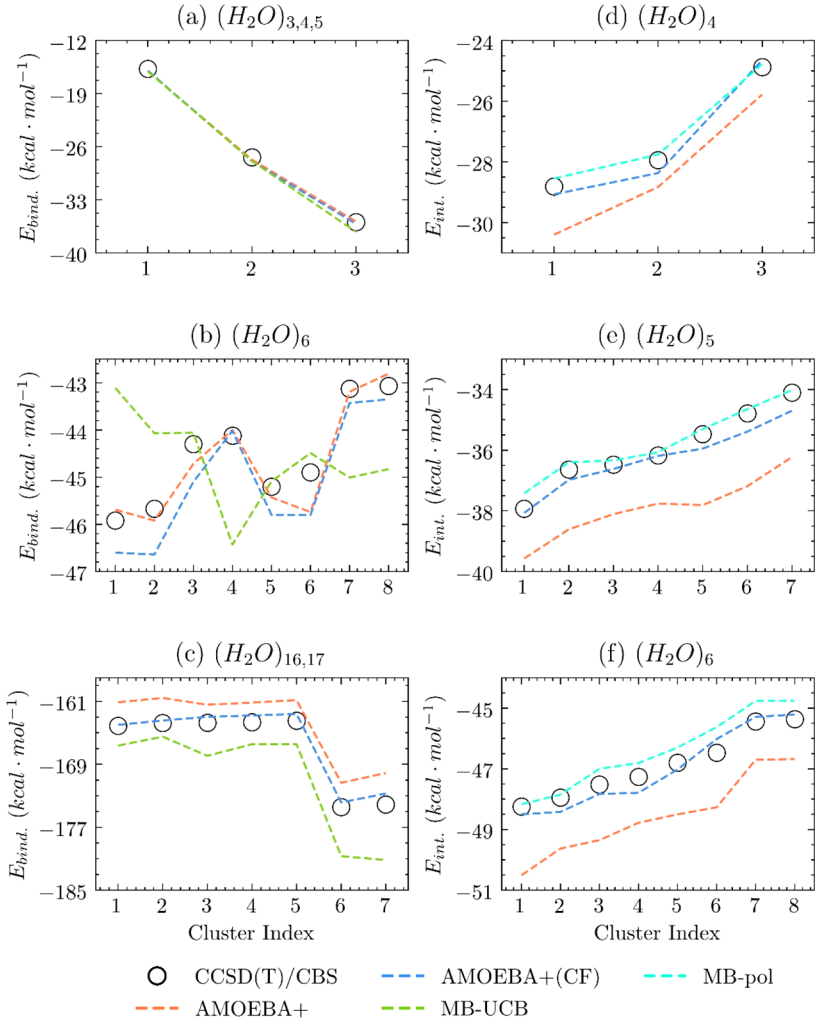

Figure 2. BEs and IEs computed with water models compared with available ab initio CCSD(T)/CBS data. (a–c) BEs of the water trimer to 17-mers and (d–f) IEs of water tetramer, pentamer, and hexamer conformers. The BEs from MB-UCB[39] and IEs from MB-pol[41] water models are provided for comparison. The numerical data, cluster indices, and references are provided in Tables S2 and S3.

DOI: 10.1021/acs.jpclett.9b03489
J. Phys. Chem. Lett. 2020, 11, 419–426

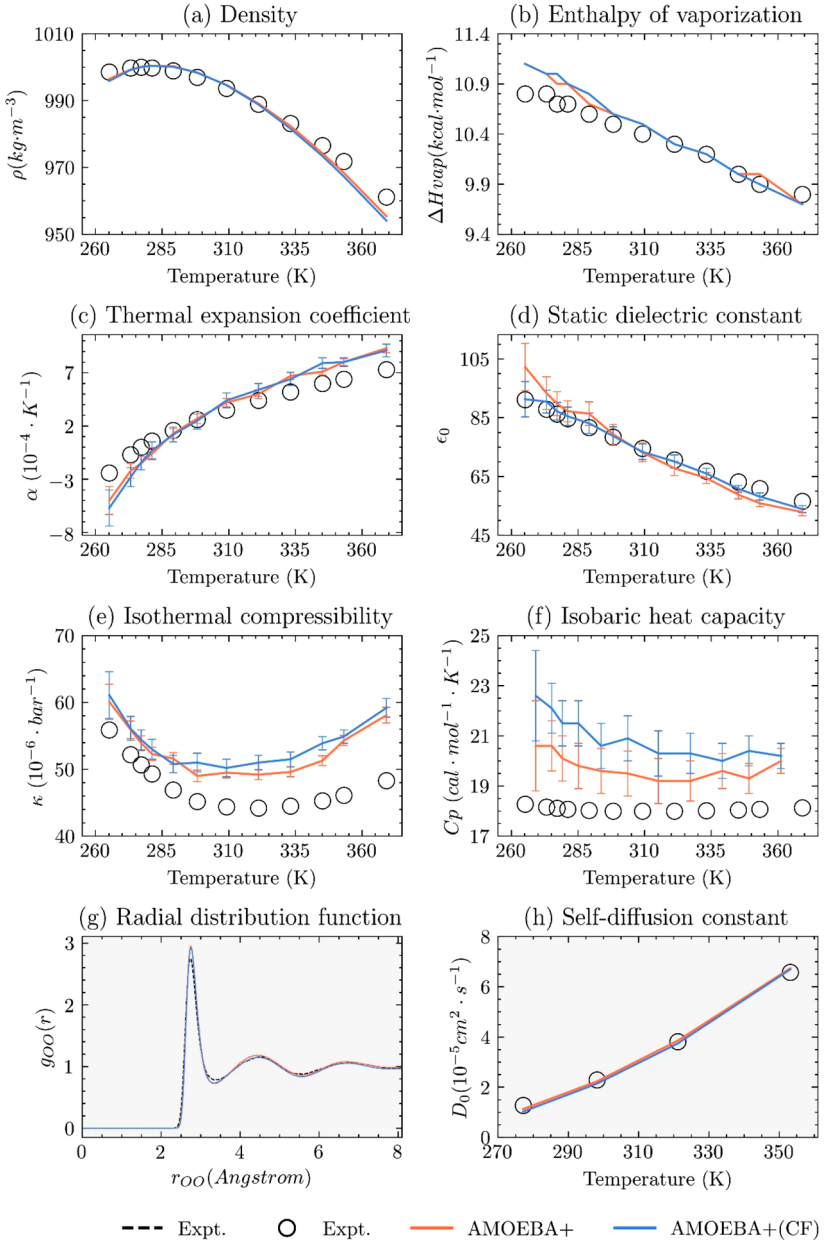

Figure 3. Liquid properties of water at a broad range of temperatures and 1 atm pressure. Properties in (a–f) were included in the ForceBalance optimization, while those in (g–h) were not used in parametrization. Error bars are also plotted if they are notable. The radial distribution functions of oxygen–hydrogen and hydrogen–hydrogen pairs are provided in Figure S2.

These results further indicate the importance of a correct monomer geometry for a flexible water model to accurately capture the complicated energy surfaces of water clusters.

Liquid Properties. As shown above, the addition of CF to AMOEBA+ significantly improves its ability to describe the structural and energetic properties of gas-phase water clusters. Here we examine the performance of AMOEBA+(CF) in liquid. Overall, the AMOEBA+(CF) model maintains the quality of the AMOEBA+ model on predicting the average thermodynamic, structural, and dynamic properties over a broad range of temperatures (Figure 3). For six thermodynamic properties included in the parametrization targets, the density (Figure 3a), enthalpy of vaporization (Figure 3b), thermal expansion coefficient (Figure 3c), and isothermal compressibility (Figure 3e), AMOEBA+(CF) captures the experimental properties as well as the previous AMOEBA+ model. The AMOEBA+(CF) liquid water density at room temperature is 997.4 ± 0.1 kg/m^3, almost exactly the same as the experimental measurement (997.0 kg/m^3), when a larger box of 60 Å^3 and a van der Waals cutoff of 12 Å are used. At 298 K, AMOEBA+(CF) is slightly worse than the AMOEBA+ model by 1.0 cal/mol/K on predicting the isobaric heat capacity (Figure 3f), which is known to be difficult for flexible classical water models due to the nuclear quantum effect.[42] AMOEBA+(CF) notably improves the agreement with experiment for the static dielectric constant in the whole temperature range compared to AMOEBA+ (Figure 3d). This can be attributed to a better quality of electrostatics, including CF-augmented multipole moments and polarizability of the AMOEBA+(CF) model, compared to AMOEBA+ (Table 1). At ambient conditions (298 K, 1 atm), AMOEBA+(CF) results in a static dielectric constant of 78.8 ± 3.1, in excellent

DOI: 10.1021/acs.jpclett.9b03489
J. Phys. Chem. Lett. 2020, 11, 419–426

agreement with the experiment (78.4). The liquid properties that were not included in the parametrization targets are also well reproduced by the AMOEBA+(CF) model, as shown in Figures 3g and S2 (SI) for the radial distribution function at ambient conditions and Figure 3h for the self-diffusion constant at a series of temperatures (also Figure S3 and Table S4). The average O−H bond length and H−O−H angle in liquid by AMOEBA+(CF) are 0.96 Å and 105.5° ± 4.7°, while experimental values are 0.97 Å and 106.1° ± 1.8°.[32] Coincidently, the AMOEBA+(CF) liquid HOH angle is consistent with the value of ab initio MD simulations (105.5°).[43] By contrast, AMOEBA+ gives an appropriate average angle (106.3° ± 4.7°) but shorter bond length (0.95 Å) in liquid (also in clusters, as shown by Hughes et al.[44]). It is worth noting that, although both water models correctly predict the average angle, as mentioned above, the AMOEBA+ angle originates from an artificially large equilibrium angle parameter (108.8°), while the AMOEBA+(CF) water automatically expands from 104.5° in isolation to 105.5° in liquid due to CF. The average amount of charges transferred for a water molecule due to the geometrical deviation is only −0.0031 *e* on the oxygen atom, of which −0.0040 *e* is contributed from angle bending, +0.0004 *e* from symmetrical bond stretching, and +0.0005 *e* from asymmetrical bond stretching.

Infrared Spectra of Liquid Water. It has been shown by the SDFF water model that CF is necessary to describe the dipole surface and vibrational spectra.[15] It is also observed that iAMOEBA fails to predict the correct relative intensity of experimental infrared (IR) spectra.[45] To investigate the impact of CF on the liquid IR spectra, we examined several AMOEBA-based water models either with or without CF. IR spectra were obtained within linear response theory through Fourier transforms of time correlation of the net dipole (simulation details in the SI). To compare with experimental IR spectra, corrections accounting for quantum effects were added to the calculated IR intensity by using a previously suggested approach.[46] Figure 4 clearly indicates that without CF

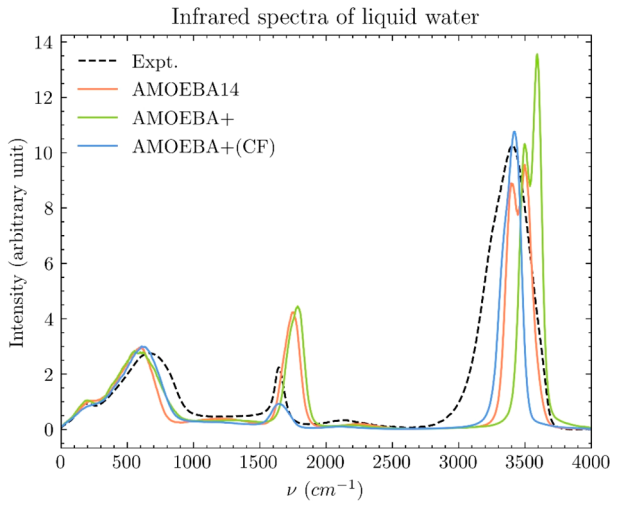

Figure 4. IR spectra of liquid water calculated with water models with/without CF and compared to the experiment. Experimental data were taken from the literature of ambient conditions (298 K and 1 atm).[49] Quantum corrections were added to each calculated spectrum using the same approach as that suggested by a previous study.[46] More simulation details are provided in the SI.

implementation both AMOEBA14 and AMOEBA+ models predict a higher bending peak (~1600 cm^{-1}) than the libration peak (~480 cm^{-1}), which was similarly observed for the AMOEBA03 water (Figure S4) and iAMOEBA models.[45] By contrast, AMOEBA+(CF) reduces the height of the bending peak and results in correct relative intensity compared to the experiment. In the OH stretching region, it is seen that the stretching is shifted to low frequencies (blue shift) from 3755 cm^{-1} (asymmetric) and 3656 cm^{-1} (symmetric) of an isolated water molecule (Table 1) to ~3550 cm^{-1} (Figure S4). This blue shift magnitude is insufficient compared to experiment, which can be attributed to the lack of explicit treatment of the nuclear quantum effect in this high-frequency region for classical models.[47,48] With an adjusted bond stretching force constant, the AMOEBA+(CF) model is able to predict the correct peak position (~3400 cm^{-1}). Additionally, it is clear that a "stiffer" bond stretching force constant also helps to prevent the peak splitting observed in AMOEBA+(CF) using a gas-phase force constant, as well as other models (Figures 4 and S4). Thus, this modified model is suggested for vibrational spectroscopy simulation in water. This modification on the bond stretching force constant has no effect on the average liquid thermodynamic or dynamic properties that we have computed.

Ice Properties. Three crystal forms of ice, Ih, Ic, and II, were simulated at 1 atm pressure and experimental temperatures by employing AMOEBA+ and AMOEBA+(CF) water models. The computational details are provided in the SI, and the results are summarized in Tables S11 and S12. The average density simulated by our models agrees reasonably well with experiment within ~2% for Ih, ~4% for Ic, and ~6% for ice II (Table S11), which can be attributed to two factors: (1) the lack of a nuclear quantum effect, which normally leads to a reduction of the simulated density, and (2) the exclusion of solid-phase properties in our parametrization. As shown in Table S12, the AMOEBA+(CF) model shows reasonable capability to predict other properties of ice Ih without explicitly parametrizing to ice data. For example, the simulated enthalpy of sublimation for ice Ih at 269 K and 1 atm is −12.13 kcal/mol, which excellently agrees with experiment (−12.20 kcal/mol).[50] By contrast, TTM-family models overpredict the enthalpy of sublimation of ice Ih, with TTM4-F being −14.40 kcal/mol and TTM2-F being −13.39 kcal/mol.[51] The average intermolecular OO distance (2.73 Å) is ~1% shorter than the experimental value (2.76 Å), which is consistent with slightly higher simulated density. The intramolecular OH distance (0.97 Å) is in agreement with experiment (0.98 Å).[52] The experimental value of the HOH angle is commonly referenced as an ideal tetrahedral angle of 109.5°. A trend of HOH angle expansion (monomer < liquid < ice) consistent with experiment is observed for the AMOEBA+(CF) model in three phases, while the AMOEBA+ model gives the opposite trend as monomer > liquid > ice.

In summary, we implemented the GDCF model into the multipole-based polarizable AMOEBA+ potential. The GDCF model was originally proposed by Dinur and Hagler and examined on small organic molecules within the point charge electrostatic framework.[20] In this work, we integrated the GDCF model with atomic multipole electrostatics (with permanent multipoles up to quadrupole) and many-body atomic dipole polarization in the AMOEBA+ framework. The energy and force expressions due to the inclusion of GDCF were derived. We examined the impact of GDCF by updating

DOI: 10.1021/acs.jpclett.9b03489
J. Phys. Chem. Lett. 2020, 11, 419−426

the AMOEBA+ water model. Our results indicate that GDCF allows the use of an appropriate equilibrium angle and bond length for an isolated water molecule, which will spontaneously adjust to the correct values in liquid. The correct monomer geometry and GDCF lead to noticeable improvements in both the BEs and IEs of water clusters. Finally, the AMOEBA+(CF) water model shows excellent liquid properties along with improved IR spectra in terms of capturing the relative intensity of bending and libration peaks.

The preliminary implementation of AMOEBA+(CF) was finished on our developing version of Tinker (CPU) and Tinker-OpenMM (GPU). MD simulations under *NVE* ensemble were carried out on both CPU and GPU codes to evaluate the energy conservation of the AMOEBA+(CF) model (simulation details in the SI). To take advantage of the double precision of the Tinker CPU code, simulation using a very tight induced dipole convergence (polar-eps 10^{-12} D) with the iterative SCF method leads to only −0.01 kcal/mol/ns of total energy drift (out of ∼−3800 kcal/mol) (Figure S5a). Alternatively, simulation with the "OPT4" extrapolated polarization scheme[53] on a CPU gives a total energy drift of −0.03 kcal/mol/ns (Figure S5b). As expected, simulations on the Tinker-OpenMM GPU (mixed precision) give a greater total energy drift of −0.2 kcal/mol/ns (Figure S5c) and +0.1 kcal/mol/ns (Figure S5d) for SCF (polar-eps 10^{-6} D due to single precision) and "OPT4" schemes, respectively. These results indicate the excellent energy conservation of our implementation. Besides, it is shown that a negligible additional cost (less than 1%) arises from the GDCF algorithms. Further code implementation and optimization in the latest version of Tinker,[54] Tinker-OpenMM,[55] and Tinker-HP[56] are ongoing, as well as the parametrization of AMOEBA+(CF) for a wide range of molecular systems.

METHODOLOGIES

Here we briefly describe the theoretical methodologies of CF implementation. The AMOEBA+ potential adopts atomic multipoles to represent atomic charge distributions, with a short-range penetration effect.[25] Multipole moments on atom i can be expressed as

$$M_i = [q, \mu_x, \mu_y, \mu_z, \Theta_{xx}, ...] \tag{3}$$

To implement the GDCF model, we followed the algorithms proposed by Dinur and Hagler[20] by including only the bond and angle contributions. For a pair of bonded atoms a and b, CFs on atoms a and b due to bond stretching are expressed as

$$dq_a = -dq_b = j_b(r_{ab} - r_{ab}^0) \tag{4}$$

where r_{ab} and r_{ab}^0 are the actual and equilibrium bond lengths; j_b is the determining parameter specific to this bond. The CF direction rule is kept the same as that in previous work.[20] Briefly, $-dq$ is added to the (1) atom with a bigger atomic number; (2) atom with more connections if rule (1) is not applicable; (3) atom with more connected hydrogen atoms if both (1) and (2) are not applicable. For an angle $\angle abc$, the CFs due to angle bending are expressed as

$$dq_a = j_{\theta 1}(\theta - \theta_0) + j'_{b1}(r_{bc} - r_{bc}^0) \tag{5}$$

$$dq_c = j_{\theta 2}(\theta - \theta_0) + j'_{b2}(r_{ab} - r_{ab}^0) \tag{6}$$

$$dq_b = -(dq_a + dq_c) \tag{7}$$

where θ and θ_0 are actual and equilibrium angle values; the second terms on the right side are due to asymmetric stretching, in which case the change of r_{bc} also affects atom a. $j_{\theta 1}$, $j_{\theta 2}$, j'_{b1} and j'_{b2} are CF parameters determined by the chemistry (atom types). The initial CF parameters of water were derived by fitting to the molecular dipole surface using the MP2/aug-cc-pvtz level of theory. In ForceBalance optimization, only the j_θ is allowed to be further optimized as we found it is more sensitive to the HOH angle than the bond-related CF parameters. For organic molecules and peptides, density functional theory may be applied to calculate the molecular dipole surface, as also suggested by other researchers.[18,19]

With the CF dq_i for atomic site i determined for a given geometry, the monopole in AMOEBA+ multipole moments then is replaced by $q + dq_i$. The modified multipole is then

$$M'_i = [q + dq_i, \mu_x, \mu_y, \mu_z, \Theta_{xx}, ...] \tag{8}$$

With the above multipoles, permanent electrostatics of AMOEBA+ is calculated as

$$E_{\text{ele}} = \sum_{i,j} M'_i T^{\text{damped}} M'_j \tag{9}$$

wherein with the AMOEBA+ potential the multipole−multipole interaction T matrix is damped to account for the charge penetration effect.[25,26] The induced dipole and polarization energy are calculated in the same manner as the current AMOEBA+ model with the updated multipoles M'.

In order to use the GDCF model in MD simulations, one needs the gradient of the potential energy with respect to the atom coordinate. We found that the final form of the electrostatic and polarization forces can be expressed in the following formula

$$F_{i,\alpha}(\text{CF}) = F_{i,\alpha} + F'_{i,\alpha} \quad (\alpha = x, y, z) \tag{10}$$

The first term on the right side stands for the usual AMOEBA+ electrostatics and polarization terms with CF-updated charges. The second chain-rule term arises from CF, which explicitly depends on the internal bonds and angles. In the SI, we show that $F'_{i,a}$ can be calculated using the accumulated potential on each atom (V_i) and the derivative of CF with respect to the coordinates $\left(\frac{\partial dq_i}{\partial \alpha}\right)$. The V_i term in the AMOEBA+ framework is contributed from permanent multipoles (charge, dipole, and quadrupole) and the induced dipole. These expressions of V_i are already calculated in the AMOEBA+ potential.[25,26] In addition, because charges in our model now depend on the atomic coordinates, the extra force contribution to the Ewald self-energy appears (see detailed derivation in the SI).

ASSOCIATED CONTENT

Supporting Information

The Supporting Information is available free of charge at https://pubs.acs.org/doi/10.1021/acs.jpclett.9b03489.

Additional methodologies, figures showing intermolecular interaction energies, radial distribution functions, self-diffusion constants of different temperatures and box sizes, IR spectra of liquid water, and an energy−time plot of NVE simulations, tables providing optimal parameters of AMOEBA+ and AMOEBA+(CF) water

DOI: 10.1021/acs.jpclett.9b03489
J. Phys. Chem. Lett. 2020, 11, 419−426

models, binding energies, interaction energies, size-corrected self-diffusion constants, liquid densities, enthalpies of vaporization, thermal expansion coefficients, isothermal compressibilities, isobaric heat capacities, static dielectric constants, densities of three forms of ice, and simulated geometrical and energetic properties of ice Ih, and additional references (PDF)

AUTHOR INFORMATION

Corresponding Author

*E-mail: pren@utexas.edu.

ORCID

Chengwen Liu: 0000-0002-3930-7793
Jean-Philip Piquemal: 0000-0001-6615-9426
Pengyu Ren: 0000-0002-5613-1910

Notes

The authors declare no competing financial interest.
All code is available in the publicly accessible TinkerTools Github site as the Tinker/AMOEBA+CF and Tinker-OpenMM/AMOEBA+CF branch.

ACKNOWLEDGMENTS

The authors are grateful for support by the Robert A. Welch Foundation (F-1691), National Institutes of Health (R01GM106137 and R01GM114237), the Cancer Prevention and Research Institute of Texas (RP160657), the National Science Foundation (CHE-1856173), and the European Research Council (ERC) under the European Union's Horizon 2020 research and innovation program (Grant Agreement No. 810367), Project EMC2.

REFERENCES

(1) Hagler, A. T. Force field development phase II: Relaxation of physics-based criteria··· or inclusion of more rigorous physics into the representation of molecular energetics. *J. Comput.-Aided Mol. Des.* **2019**, *33* (2), 205.
(2) Lemkul, J. A.; Huang, J.; Roux, B.; MacKerell, A. D., Jr. An Empirical Polarizable Force Field Based on the Classical Drude Oscillator Model: Development History and Recent Applications. *Chem. Rev.* **2016**, *116* (9), 4983.
(3) Jing, Z.; Liu, C.; Cheng, S. Y.; Qi, R.; Walker, B. D.; Piquemal, J.-P.; Ren, P. Polarizable Force Fields for Biomolecular Simulations: Recent Advances and Applications. *Annu. Rev. Biophys.* **2019**, *48*, 371.
(4) Patel, S.; Brooks, C. L. Fluctuating charge force fields: recent developments and applications from small molecules to macromolecular biological systems. *Mol. Simul.* **2006**, *32* (3−4), 231.
(5) Patel, S.; Brooks, C. L., III CHARMM fluctuating charge force field for proteins: I parameterization and application to bulk organic liquid simulations. *J. Comput. Chem.* **2004**, *25* (1), 1.
(6) Patel, S.; Mackerell, A. D., Jr.; Brooks, C. L., III CHARMM fluctuating charge force field for proteins: II Protein/solvent properties from molecular dynamics simulations using a nonadditive electrostatic model. *J. Comput. Chem.* **2004**, *25* (12), 1504.
(7) Poier, P. P.; Jensen, F. Describing Molecular Polarizability by a Bond Capacity Model. *J. Chem. Theory Comput.* **2019**, *15* (5), 3093.
(8) Benedict, W. S.; Gailar, N.; Plyler, E. K. Rotation-Vibration Spectra of Deuterated Water Vapor. *J. Chem. Phys.* **1956**, *24* (6), 1139.
(9) Ichikawa, K.; Kameda, Y.; Yamaguchi, T.; Wakita, H.; Misawa, M. Neutron-diffraction investigation of the intramolecular structure of a water molecule in the liquid phase at high temperatures. *Mol. Phys.* **1991**, *73* (1), 79.
(10) Kuhs, W. F.; Lehmann, M. S. The structure of the ice Ih by neutron diffraction. *J. Phys. Chem.* **1983**, *87* (21), 4312.
(11) Fanourgakis, G. S.; Xantheas, S. S. The bend angle of water in ice Ih and liquid water: The significance of implementing the nonlinear monomer dipole moment surface in classical interaction potentials. *J. Chem. Phys.* **2006**, *124* (17), 174504.
(12) Dinur, U. "Flexible" water molecules in external electrostatic potentials. *J. Phys. Chem.* **1990**, *94* (15), 5669.
(13) Palmo, K.; Mannfors, B.; Mirkin, N. G.; Krimm, S. Inclusion of charge and polarizability fluxes provides needed physical accuracy in molecular mechanics force fields. *Chem. Phys. Lett.* **2006**, *429* (4), 628.
(14) Palmo, K.; Mannfors, B.; Krimm, S. Balanced charge treatment of intramolecular electrostatic interactions in molecular mechanics energy functions. *Chem. Phys. Lett.* **2003**, *369* (3), 367.
(15) Mannfors, B.; Palmo, K.; Krimm, S. Spectroscopically Determined Force Field for Water Dimer: Physically Enhanced Treatment of Hydrogen Bonding in Molecular Mechanics Energy Functions. *J. Phys. Chem. A* **2008**, *112* (49), 12667.
(16) Burnham, C. J.; Xantheas, S. S. Development of transferable interaction models for water. IV. A flexible, all-atom polarizable potential (TTM2-F) based on geometry dependent charges derived from an ab initio monomer dipole moment surface. *J. Chem. Phys.* **2002**, *116* (12), 5115.
(17) Fanourgakis, G. S.; Xantheas, S. S. Development of transferable interaction potentials for water. V. Extension of the flexible, polarizable, Thole-type model potential (TTM3-F, v. 3.0) to describe the vibrational spectra of water clusters and liquid water. *J. Chem. Phys.* **2008**, *128* (7), 074506.
(18) Sedghamiz, E.; Nagy, B.; Jensen, F. Probing the Importance of Charge Flux in Force Field Modeling. *J. Chem. Theory Comput.* **2017**, *13* (8), 3715.
(19) Sedghamiz, E.; Ghalami, F. Evaluating the Effects of Geometry and Charge Flux in Force Field Modeling. *J. Phys. Chem. A* **2018**, *122* (19), 4647.
(20) Dinur, U.; Hagler, A. T. Geometry-dependent atomic charges: Methodology and application to alkanes, aldehydes, ketones, and amides. *J. Comput. Chem.* **1995**, *16* (2), 154.
(21) Ren, P. Y.; Ponder, J. W. Polarizable atomic multipole water model for molecular mechanics simulation. *J. Phys. Chem. B* **2003**, *107* (24), 5933.
(22) Shi, Y.; Xia, Z.; Zhang, J.; Best, R.; Wu, C.; Ponder, J. W.; Ren, P. Polarizable Atomic Multipole-Based AMOEBA Force Field for Proteins. *J. Chem. Theory Comput.* **2013**, *9* (9), 4046.
(23) Zhang, C.; Bell, D.; Harger, M.; Ren, P. Polarizable Multipole-Based Force Field for Aromatic Molecules and Nucleobases. *J. Chem. Theory Comput.* **2017**, *13* (2), 666.
(24) Ponder, J. W.; Wu, C.; Ren, P.; Pande, V. S.; Chodera, J. D.; Schnieders, M. J.; Haque, I.; Mobley, D. L.; Lambrecht, D. S.; DiStasio, R. A., Jr.; Head-Gordon, M.; Clark, G. N.; Johnson, M. E.; Head-Gordon, T. Current status of the AMOEBA polarizable force field. *J. Phys. Chem. B* **2010**, *114* (8), 2549.
(25) Rackers, J. A.; Wang, Q.; Liu, C.; Piquemal, J.-P.; Ren, P.; Ponder, J. W. An optimized charge penetration model for use with the AMOEBA force field. *Phys. Chem. Chem. Phys.* **2017**, *19* (1), 276.
(26) Liu, C.; Piquemal, J.-P.; Ren, P. AMOEBA+ Classical Potential for Modeling Molecular Interactions. *J. Chem. Theory Comput.* **2019**, *15* (7), 4122.
(27) Liu, C.; Qi, R.; Wang, Q.; Piquemal, J. P.; Ren, P. Capturing Many-Body Interactions with Classical Dipole Induction Models. *J. Chem. Theory Comput.* **2017**, *13* (6), 2751.
(28) Thole, B. T. Molecular Polarizabilities Calculated with a Modified Dipole Interaction. *Chem. Phys.* **1981**, *59* (3), 341.
(29) van Duijnen, P. T.; Swart, M. Molecular and Atomic Polarizabilities: Thole's Model Revisited. *J. Phys. Chem. A* **1998**, *102* (14), 2399.
(30) Qi, R.; Wang, Q.; Ren, P. General van der Waals potential for common organic molecules. *Bioorg. Med. Chem.* **2016**, *24* (20), 4911.
(31) Wang, L. P.; Martinez, T. J.; Pande, V. S. Building Force Fields: An Automatic, Systematic, and Reproducible Approach. *J. Phys. Chem. Lett.* **2014**, *5* (11), 1885.

DOI: 10.1021/acs.jpclett.9b03489
J. Phys. Chem. Lett. 2020, 11, 419−426

(32) Ben-Naim, A. *Molecular Theory of Water and Aqueous Solutions*; World Scientific, 2011.
(33) Clough, S. A.; Beers, Y.; Klein, G. P.; Rothman, L. S. Dipole moment of water from Stark measurements of H_2O, HDO, and D_2O. *J. Chem. Phys.* **1973**, *59* (5), 2254.
(34) Verhoeven, J.; Dymanus, A. Magnetic Properties and Molecular Quadrupole Tensor of the Water Molecule by Beam-Maser Zeeman Spectroscopy. *J. Chem. Phys.* **1970**, *52* (6), 3222.
(35) Murphy, W. F. The Rayleigh depolarization ratio and rotational Raman spectrum of water vapor and the polarizability components for the water molecule. *J. Chem. Phys.* **1977**, *67* (12), 5877.
(36) Maroulis, G. Hyperpolarizability of H_2O revisited: accurate estimate of the basis set limit and the size of electron correlation effects. *Chem. Phys. Lett.* **1998**, *289* (3−4), 403.
(37) Tschumper, G. S.; Leininger, M. L.; Hoffman, B. C.; Valeev, E. F.; Schaefer, H. F.; Quack, M. Anchoring the water dimer potential energy surface with explicitly correlated computations and focal point analyses. *J. Chem. Phys.* **2002**, *116* (2), 690.
(38) Smith, B. J.; Swanton, D. J.; Pople, J. A.; Schaefer, H. F.; Radom, L. Transition structures for the interchange of hydrogen atoms within the water dimer. *J. Chem. Phys.* **1990**, *92* (2), 1240.
(39) Das, A. K.; Urban, L.; Leven, I.; Loipersberger, M.; Aldossary, A.; Head-Gordon, M.; Head-Gordon, T. Development of an Advanced Force Field for Water Using Variational Energy Decomposition Analysis. *J. Chem. Theory Comput.* **2019**, *15* (9), 5001.
(40) Laury, M. L.; Wang, L. P.; Pande, V. S.; Head-Gordon, T.; Ponder, J. W. Revised Parameters for the AMOEBA Polarizable Atomic Multipole Water Model. *J. Phys. Chem. B* **2015**, *119* (29), 9423.
(41) Reddy, S. K.; Straight, S. C.; Bajaj, P.; Pham, C. H.; Riera, M.; Moberg, D. R.; Morales, M. A.; Knight, C.; Götz, A. W.; Paesani, F. On the accuracy of the MB-pol many-body potential for water: Interaction energies, vibrational frequencies, and classical thermodynamic and dynamical properties from clusters to liquid water and ice. *J. Chem. Phys.* **2016**, *145* (19), 194504.
(42) Vega, C.; Conde, M. M.; McBride, C.; Abascal, J. L. F.; Noya, E. G.; Ramirez, R.; Sesé, L. M. Heat capacity of water: A signature of nuclear quantum effects. *J. Chem. Phys.* **2010**, *132* (4), 046101.
(43) Silvestrelli, P. L.; Parrinello, M. Structural, electronic, and bonding properties of liquid water from first principles. *J. Chem. Phys.* **1999**, *111* (8), 3572.
(44) Hughes, Z. E.; Ren, E.; Thacker, J. C. R.; Symons, B. C. B.; Silva, A. F.; Popelier, P. L. A. A FFLUX Water Model: Flexible, Polarizable and with a Multipolar Description of Electrostatics. *J. Comput. Chem.* **2019**, DOI: 10.1002/jcc.26111.
(45) Wang, L. P.; Head-Gordon, T.; Ponder, J. W.; Ren, P.; Chodera, J. D.; Eastman, P. K.; Martinez, T. J.; Pande, V. S. Systematic improvement of a classical molecular model of water. *J. Phys. Chem. B* **2013**, *117* (34), 9956.
(46) Gaigeot, M.-P.; Sprik, M. Ab Initio Molecular Dynamics Computation of the Infrared Spectrum of Aqueous Uracil. *J. Phys. Chem. B* **2003**, *107* (38), 10344.
(47) Medders, G. R.; Paesani, F. Infrared and Raman Spectroscopy of Liquid Water through "First-Principles" Many-Body Molecular Dynamics. *J. Chem. Theory Comput.* **2015**, *11* (3), 1145.
(48) Kapil, V.; VandeVondele, J.; Ceriotti, M. Accurate molecular dynamics and nuclear quantum effects at low cost by multiple steps in real and imaginary time: Using density functional theory to accelerate wavefunction methods. *J. Chem. Phys.* **2016**, *144* (5), 054111.
(49) Maréchal, Y. The molecular structure of liquid water delivered by absorption spectroscopy in the whole IR region completed with thermodynamics data. *J. Mol. Struct.* **2011**, *1004* (1), 146.
(50) Murphy, D. M.; Koop, T. Review of the vapour pressures of ice and supercooled water for atmospheric applications. *Q. J. R. Meteorol. Soc.* **2005**, *131* (608), 1539.
(51) Burnham, C. J.; Anick, D. J.; Mankoo, P. K.; Reiter, G. F. The vibrational proton potential in bulk liquid water and ice. *J. Chem. Phys.* **2008**, *128* (15), 154519.
(52) Floriano, M. A.; Klug, D. D.; Whalley, E.; Svensson, E. C.; Sears, V. F.; Hallman, E. D. Direct determination of the intramolecular O−D distance in ice Ih and Ic by neutron diffraction. *Nature* **1987**, *329* (6142), 821.
(53) Simmonett, A. C.; Pickard, F. C., IV; Ponder, J. W.; Brooks, B. R. An empirical extrapolation scheme for efficient treatment of induced dipoles. *J. Chem. Phys.* **2016**, *145* (16), 164101.
(54) Rackers, J. A.; Wang, Z.; Lu, C.; Laury, M. L.; Lagardère, L.; Schnieders, M. J.; Piquemal, J. P.; Ren, P.; Ponder, J. W. Tinker 8: Software Tools for Molecular Design. *J. Chem. Theory Comput.* **2018**, *14* (10), 5273.
(55) Eastman, P.; Swails, J.; Chodera, J. D.; McGibbon, R. T.; Zhao, Y.; Beauchamp, K. A.; Wang, L. P.; Simmonett, A. C.; Harrigan, M. P.; Stern, C. D.; Wiewiora, R. P.; Brooks, B. R.; Pande, V. S. OpenMM 7: Rapid development of high performance algorithms for molecular dynamics. *PLoS Comput. Biol.* **2017**, *13* (7), No. e1005659.
(56) Lagardère, L.; Jolly, L. H.; Lipparini, F.; Aviat, F.; Stamm, B.; Jing, Z. F.; Harger, M.; Torabifard, H.; Cisneros, G. A.; Schnieders, M. J.; Gresh, N.; Maday, Y.; Ren, P. Y.; Ponder, J. W.; Piquemal, J. P. Tinker-HP: a massively parallel molecular dynamics package for multiscale simulations of large complex systems with advanced point dipole polarizable force fields. *Chem. Sci.* **2018**, *9* (4), 956.

DOI: 10.1021/acs.jpclett.9b03489
J. Phys. Chem. Lett. 2020, 11, 419−426